4

Computational Seismic Holography of Acoustic Waves in the Solar Interior

Charles Lindsey[1], Douglas Braun[1], Irene González Hernández[2] and Alina Donea[3]
[1]*NorthWest Research Associates*
[2]*National Solar Observatory*
[3]*Monash University*
[1,2]*USA*
[3]*Australia*

1. Introduction

1.1 Helioseismology

The advent of solar seismology is widely recognized as the independent discoveries by Leighton, Noyes & Simon (1963) and Evans, Michard & Servajean (1962) of Doppler oscillations in the Sun's surface, mostly with periods ranging from about 2 to 8 minutes. This was recognized as the surface signature of waves traveling beneath the Sun's surface. These waves, now understood to be generated by convection a few hundred km beneath the Sun's surface (Stein et al. , 2004), penetrate deep beneath the surface, filling the solar interior. The idea of using observations of these waves as a diagnostic of the Sun's interior structure was introduced by Ulrich (1970), and developed at length by Deubner (1975) and Rhodes, Ulrich & Simon (1977). Continued development followed many different avenues, some of these similar in some ways to geoseismic diagnostics of the Earth's interior. Indeed, helioseismic holography and "migration theory", the latter developed by Claerbout (1970) for applications in geoseismology, share basic concepts in wave optics in very similar contexts. However, solar seismology has overwhelming advantages, both in the quality, extent and uniformity of the observations and in the optical quality of the solar interior as an acoustic medium. Solar seismology gave us maps of the solar interior rotation rate (Rhodes, Deubner & Ulrich , 1979), affirming that the Sun is a differentially rotating fluid, its convection zone continuously being warped as the equatorial region rotates significantly faster than the inner polar region and the outer equatorial convection zone rotates faster than the deep convection zone. Helioseismology is also the significant observational basis of our present understanding of the thermal structure of the solar interior in standard models such as Christensen-Dalsgaard, Proffitt & Thompson (1993).

Solar seismology has been largely developed along two significantly separate lines. What is now generally recognized as "global helioseismology" views the Sun as a system of harmonic oscillators and relies heavily on the frequencies of its thousands of normal modes to build a model of the general thermal structure of the Sun and how different layers of it rotate. These diagnostics give us significant discrimination in depth and some in latitude, but none in longitude. What is recognized as "local helioseismology" uses perspectives that tend to be more familiar to optics to focus on relatively compact regions. The local discrimination our

eyesight gives us is a benefit of a *phase coherence* that is preserved in the medium through which the light we see propagates. Coherence is a crucial benefit to all aspects of solar seismology as well.

Following developments by Zernike (1938) and van Cittert (1939), coherence has come to be formally expressed by a complex "mutual coherence function",

$$\Gamma(\mathbf{r},\ \mathbf{r}',\ \tau)\ =\ \langle \psi(\mathbf{r},\ t)\psi^*(\mathbf{r}',\ t\ +\ \tau)\rangle, \tag{1}$$

correlating complex wave amplitudes $\psi(\mathbf{r},\ t)$ and $\psi(\mathbf{r}',\ t\ +\ \tau)$ at points $\mathbf{r}$ and $\mathbf{r}'$ in space, where the angular brackets indicate an averaging of their contents over time, t (see Born & Wolf , 1975a).[1] This has a strong analogy in a broad spectrum of diagnostic techniques in local helioseismology called "time-distance helioseismology" (Duvall et al. , 1993). Computational seismic holography is among these techniques, and can be expressed in terms of mutual coherence functions. The mutual coherence function, $\Gamma(\mathbf{r},\ \mathbf{r}',\ \tau)$, offers a statistical facsimile of ψ itself where optical technology is insufficiently fast to capture and record the temporal variations of ψ directly. The heart of this facsimile is in that $\Gamma(\mathbf{r},\ \mathbf{r}',\ \tau)$ obeys the same wave equation as ψ, in both $(\mathbf{r},\ \tau)$-space and $(\mathbf{r}',\ \tau)$-space.

A powerful technique in electromagnetic optics for deriving information on $\Gamma(\mathbf{r},\ \mathbf{r}',\ \tau)$—and fundamental to the development of electromagnetic holography—has been the superposition of electromagnetic fields, $\psi(\mathbf{r},\ t)$ and $\psi(\mathbf{r}',\ t')$, nominally destined to arrive at separates points, $\mathbf{r}$ and $\mathbf{r}'$, at separate times, t and t', onto the same region at the same time, so that they interfere. The resulting interference fringes, give us phase information about Γ that registers on a photographic plate, a medium normally sensitive only to intensity, not phase. The development of electromagnetic holography in the 1960s used this interference-based technique very effectively, benefiting from the long coherence lengths of monochromatic radiation from lasers.

The major practical difference between helioseismology and the electromagnetic optics familiar to electromagnetic holography is our ability, in the case of the former, to map the wave-mechanical field, ψ, in temporal detail as well as spatial, sampling it several times over its acoustic period, $2\pi/\omega$, over most of the Sun's visible hemisphere for weeks, even months, with infrequent interruptions. Also relevant is that acoustic radiation in the solar interior is highly polychromatic; its coherence length is less than the mean wavelength of the acoustic spectrum. However, having a clear temporal record of ψ covering a large fraction of the Sun's surface circumvents the need for a statistical facsimile of ψ, such as Γ, to determine phase-coherent extrapolations of either ψ or Γ into a wave-mechanical medium. The extrapolation can simply be applied to ψ directly, according to the laws of wave mechanics as we understand them. Moreover, we can do this not just at a single monochromatic frequency but over the entire acoustic spectrum accessible to helioseismic observations. This turns out to be a great benefit, since the times required to accumulate statistics at minutes-long helioseismic periods are much greater than for the femtosecond periods of visible light.

[1] In standard optics, the complex field amplitude $\psi(\mathbf{r},\ t)$ is an analytic extension of respective real amplitudes $\psi^r(\mathbf{r},\ t)$ that in principle might could be measured and recorded in terms of real values, the former obtained by inverting the Fourier transform, $\hat{\psi}(\mathbf{r},\ \omega)$, of $\psi^r(\mathbf{r},\ t)$, but truncating the negative frequencies, ω, hence,

$$\psi(\mathbf{r},\ t)\ \equiv\ \frac{2}{\sqrt{2\pi}}\int_0^\infty\ \hat{\psi}(\mathbf{r},\ \omega)\ e^{i\omega t}\ d\omega. \tag{2}$$

The analytic extension, then, is a complex extension of the real-valued amplitude of which the real-valued amplitude is the real part: $\psi^r(\mathbf{r},\ t) = \mathrm{Re}\{\psi(\mathbf{r},\ t)\}$.

Computational holography of helioseismic observations, then, is not based on any facsimile of the superposed monochromatic reference beams familiar to electromagnetic holography. The lack of such a facsimile has made it somewhat unfamiliar to some interpreters of electromagnetic holography. However, the object is the same: the extrapolation of some phase-coherent attribute of the wave-mechanical field, ψ, from the surface that samples it a macroscopic distance therefrom, based on a phase-informative record of the signature ψ manifests at the sampling surface. This idea was first proposed by Roddier (1975). It was later re-introduced by Lindsey & Braun (1990) as a proposed means of viewing solar activity in the Sun's far hemisphere, i.e., viewing it acoustically from the near hemisphere through the intervening interior medium. Further developments are described by Braun et al. (1992), Lindsey et al. (1996) and Lindsey & Braun (1997), the latter expressing seismic holography in the context of the more-recently introduced time-distance helioseismology (Duvall et al. , 1993; 1996), and by Chang et al. (1997), Braun & Lindsey (1998), Lindsey & Braun (2000a), Chou (2000), and Lindsey & Braun (2000b).

The technical ability to accomplish holographic extrapolations without recourse to the coherence function, Γ, does not detract in any way from the usefulness of Γ in solar seismology. On the contrary, the temporal discrimination helioseismic recordings of ψ give us allows us to compute $\Gamma(\mathbf{r},\ \mathbf{r}',\ \tau)$ directly from ψ without recourse to superposition and interference on a medium that is sensitive only to intensity. This is a major element of time-distance helioseismology, upon which the development of helioseismic holography has drawn heavily (Lindsey & Braun , 1997; 2000b), and of which of helioseismic holography can now conveniently be regarded as substantially a chapter.

1.2 Basic principles of solar acoustic holography

The computational technique upon which helioseismic holography is based is best expressed in the context of a simple example, introduced by Lindsey & Braun (2000b). Consider an ideal acoustic medium, such as we suppose the solar interior to approach, with one or more monopolar acoustic emitters submerged into it. Figure 1 illustrates such a scenario with two such sources, monochromatic in this instance, at significantly different depths, representing surfaces of constant phase at a particular instant as wave fronts. The only visible manifestation of this acoustic field, $\psi(\mathbf{r},\ t)$, is the disturbances that appear at the solar surface, $\mathcal{S}_0$, which generally first appear at the point on $\mathcal{S}_0$ directly above the source whose issue they represent and propagate outward along $\mathcal{S}_0$ therefrom. The motion of these disturbances across $\mathcal{S}_0$ is the basic content of helioseismic observations of the solar surface in such a scenario.

Suppose now that we have a detailed record of the foregoing disturbances over some domain, $\mathcal{R}$, of $\mathcal{S}_0$ for a period of at least a few oscillatory periods. Elementary computational acoustic holography consists of the following exercise:

1. applying these disturbances in some domain, $\mathcal{P} \in \mathcal{S}_0$, *in time reverse* to the surface, $\mathcal{S}_0$, of an *acoustic model* of the solar medium that itself is devoid of sources, absorbers or other significant anomalies,
2. allowing the model to propagate the resulting disturbances backwards into its interior, and
3. sampling the regressed acoustic field in some domain within the model.

Figure 2 illustrates steps 2 and 3 for the instance of a sampling domain that is a surface, $\mathcal{S}_z$, of constant depth, z, beneath $\mathcal{S}_0$. We call the time-reversed acoustic field, $H_+(\mathbf{r},\ t)$, in the model the "coherent acoustic egression", in that $H_+(\mathbf{r},\ t)$ represents a disturbance manifested by a wave, ψ, that had arrived at the solar surface, $\mathcal{S}_0$, with every apparent intention of egressing through it from the interior of the medium—such as in the case a medium that would provide

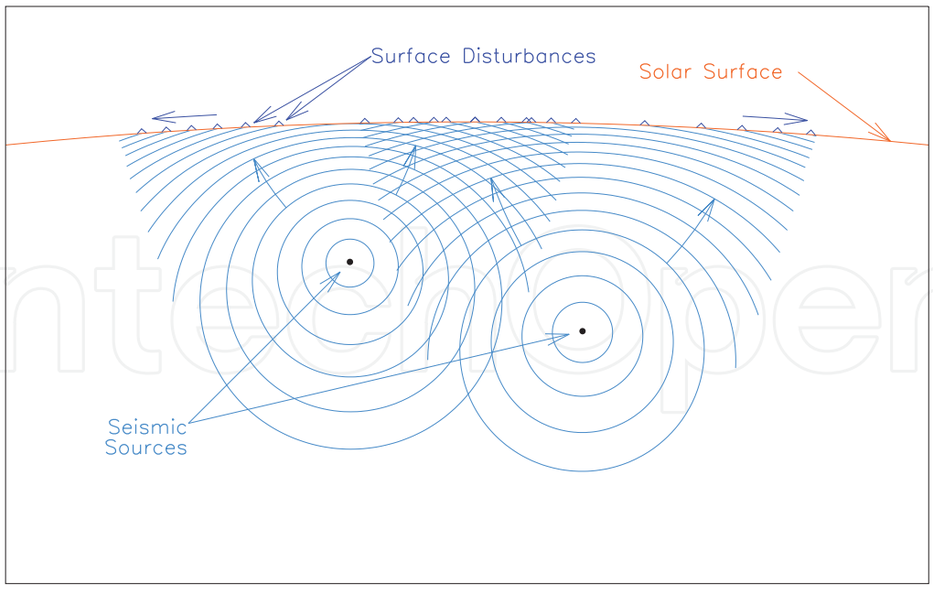

Fig. 1. Seismic waves emanating from submerged sources produce surface disturbances that propagate circularly outward along the solar surface from points directly above said sources, as indicated by generally out-going arrows.

somewhere for it to go after passing through $\mathcal{S}_0$, or in the case a surface boundary that would simply absorb it.

Once the submerged acoustic field, H_+, is recorded, a broad variety of applications are possible. The ideal analogy to what our eyes appear to give us, or a photographic plate, is the mean acoustic power. When such an averaging is applied directly to the acoustic field, ψ, we see at the solar surface, i.e., $\langle|\psi(\mathbf{r},\ t)|^2\rangle$, we call it an "acoustic-power map". Similarly applied to the acoustic egression, $\langle|H_+(\mathbf{r},\ t)|^2\rangle$, the result is an "egression-power map".

Based on our experience of optics, when the sampling surface sits at the depth of a source, $\langle|H_+(\mathbf{r},\ t)|^2\rangle$ should be characterized by a relatively compact signature, one that we recognize to be "in focus". This is supposedly the case for the source on the left in Figure 2, as represented by the egression-power plot at the bottom of the panel. If the sampling surface is moved substantially above or below the source depth, the signature remains extant, but spreads out of focus. Hence, when the sampling domain is a surface region, such as $\mathcal{S}_z$, we often call it "the focal surface". If $\mathcal{S}_z$ is planar in some approximation, we often call it the "focal plane". A particular point $\mathbf{r}$ in $\mathcal{S}_z$ can be called a "focal point", or simply a "focus" of the regression computation. The domain, $\mathcal{P}$, on $\mathcal{S}_0$ over which the observations, ψ, were applied in time reverse is called the "pupil" of the regression computation. In practice, it turns out to be fairly straight-forward to specify a pupil that is dependent upon the focus. This has strong advantages we will explain in the following section.

1.3 The computational task

A fundamental character of wave mechanics in a medium that preserves coherence is the possibility, at least in principle, of reconstructing, from measurements of a wave-mechanical field, ψ, in a thin surface, $\mathcal{S}$, significant information about ψ a long distance from $\mathcal{S}$—and an appropriately long time before or after the measurements. In relatively simple applications, this extrapolation is made in a medium that is relatively uniform, such as air. For simplicity, we will begin with a brief review of the concept for this case, and then extend the formalism

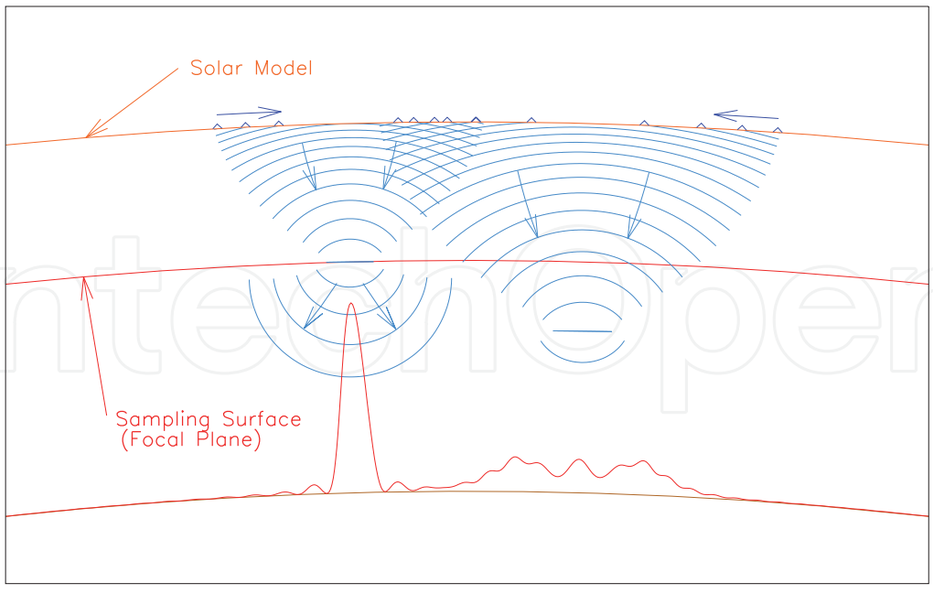

Fig. 2. Coherent computational regression of the surface acoustic field into the supposed solar interior. Surface disturbances recorded in the neighborhood overlying submerged sources are applied in time reverse to a sourceless acoustic model of the solar interior and computationally conducted back into the model interior. The underlying acoustic field differs in important respects from that actually produced by the sources. Nevertheless, a well-appropriated sampling of the regressed acoustic field renders localized sources with strong, compact signatures at appropriate depths. The seismic signature of a source that lies considerably below or above the sampling surface is rendered by a signature that is substantial but significantly out of focus.

for this to accommodate the significantly non-uniform solar interior. The former is the object of the Helmholtz-Kirchhoff integral theorem. For a formal elaboration of Helmholtz-Kirchhoff theory, we refer to Born & Wolf (1975b).

Provided an appropriately uniform medium described by a scalar wave-mechanical field, ψ, the Helmholtz-Kirchhoff integral prescribes $\psi(\mathbf{r},\ t)$ at any location, $\mathbf{r}$, in the interior of a closed region, V, and at any time, t, in terms of the values of ψ and its normal derivative, $\partial\psi/\partial n$, on the boundary, ∂V, of V in a range of "retarded times", $t_{\rm ret}$, appropriately prior to t:

$$\psi(\mathbf{r},\ t)\ =\ \int_{\partial V} d^2\mathbf{r}'\ \Big(\frac{\partial}{\partial n'}\mathcal{G}_+(\mathbf{r},\ \mathbf{r}')\ \psi(\mathbf{r}',\ t_{\rm ret})\ +\ \mathcal{G}_+(\mathbf{r},\ \mathbf{r}')\frac{\partial}{\partial n'}\ \psi(\mathbf{r}',\ t_{\rm ret})\Big), \tag{3}$$

where

$$\mathcal{G}_+(\mathbf{r},\ \mathbf{r}')\ =\ \frac{1}{4\pi|\mathbf{r}\ -\ \mathbf{r}'|}, \tag{4}$$

and

$$t_{\rm ret} \equiv t\ -\ \frac{|\mathbf{r}\ -\ \mathbf{r}'|}{c}, \tag{5}$$

with c representing the characteristic speed of propagation, supposed a constant. In preparation for the extension of this concept into a non-uniform medium, it is useful first

to write equations (3–5) in the alternative form:

$$\psi(\mathbf{r},\ t)\ =\ \int_{-\infty}^{\infty} dt' \int_{\partial V} d^2\mathbf{r}' \left(\frac{\partial}{\partial n'}\ \mathcal{G}_+(\mathbf{r},\ \mathbf{r}';\ t\ -\ t')\ \ \psi(\mathbf{r}',\ t') \right.$$
$$\left. +\ \mathcal{G}_+(\mathbf{r},\ \mathbf{r}';\ t\ -\ t')\ \frac{\partial}{\partial n'}\ \psi(\mathbf{r}',\ t') \right), \tag{6}$$

where now

$$\mathcal{G}_+(\mathbf{r},\ \mathbf{r}';\ \tau)\ =\ \frac{1}{4\pi|\mathbf{r}\ -\ \mathbf{r}'|}\ \delta\Big(\tau\ -\ \frac{|\mathbf{r}\ -\ \mathbf{r}'|}{c}\Big), \tag{7}$$

in which δ signifies the Dirac-delta function, and $\mathcal{G}_+$ the "monopolar Green's function" of the medium.

A great deal of the practical substantiality of optics can be regarded in terms of a simple adaptation of the Helmholtz-Kirchhoff integral when nothing like the entirety of ψ *or* its normal derivative are accessible over anything like the entirety of any surface enclosing the specimen we propose to look at. For example, when we use our eyes to look at a luna moth ten meters from the surfaces of our corneas, the combined solid angle subtended by the two pupils of our eyes is only a few millionths of the 4π steradians over which the moth scatters radiation that hits it. It is well known that what our eyes give us is far from a complete representation of the electromagnetic field in the neighborhood of the moth, even in the relatively uniform electromagnetic medium exterior to the moth. We nevertheless learn a remarkable amount about moths from this incomplete representation. Based on this, we generally treat the incomplete representation such as that rendered by our limited pupils to be an important component of some aspect of the electromagnetic field in the neighborhood of the moth.

Helioseismic observations give us a representation of the acoustic field, ψ, in terms of the line-of-sight component of the motion of the medium, measured by the Doppler shift in a photospheric line over the Sun's near hemisphere. Hence, we propose to express the incomplete phase-coherent regression of ψ by the application of just the left term in the large parentheses in equation (6) over a limited region, $\mathcal{P}$, of the solar surface:

$$H_+(\mathbf{r},\ t)\ \equiv\ \int_{-\infty}^{\infty} dt' \int_{\mathcal{P}} d^2\mathbf{r}'\ G_+(\mathbf{r},\ \mathbf{r}';\ t\ -\ t')\ \psi(\mathbf{r}',\ t'), \tag{8}$$

where

$$G_+(\mathbf{r},\ \mathbf{r}';\ \tau)\ \equiv\ \frac{\partial}{\partial n'}\mathcal{G}_+(\mathbf{r},\ \mathbf{r}';\ \tau). \tag{9}$$

The point $\mathbf{r}$ is the aforementioned "focus" of the acoustic regression, introduced at the end of §1.2. The region, $\mathcal{P}$, over which the integral over $d^2\mathbf{r}'$ is taken is the "pupil" introduced directly thereafter. As mentioned at the end of §1.2, the pupil can be dependent upon the focus, $\mathbf{r}$. Indeed, it is generally useful to have the pupil "follow" the focus, keeping the same relative spatial relationship to it everywhere possible, so that effects such as diffraction will be as uniform as possible.

The extension of the Helmholtz-Kirchhoff formalism to a non-uniform acoustic medium entails two significant adaptations to uniform acoustics:

1. The non-uniformity of the medium is expressed by an appropriate revision of the Green's functions, $\mathcal{G}_+$ and G_+. In the case of a uniform medium, $\mathcal{G}_+$ could be—indeed was—expressed as a function of a single scalar, $|\mathbf{r}\ -\ \mathbf{r}'|$, greatly simplifying computational logistics. This is no longer so in solar-interior acoustics. In a spherically-symmetric

medium, however, both $\mathcal{G}_+$ and G_+ can be expressed as functions of the depth of $\mathbf{r}$ and the angle between $\mathbf{r}$ and surface $\mathbf{r}'$ as projected from Sun center.

2. The solar interior is dispersive. Hence, the temporal dependencies of neither $\mathcal{G}_+$ nor G_+ are the infinitely sharp Dirac delta function expressed by equation (7).

For a discussion of means by which realistic Green's functions, $\mathcal{G}_+$ and G_+, can be determined in a medium such as the solar interior, we refer to Lindsey & Braun (2000b).
The computation of H_+ is greatly facilitated in the frequency domain of the temporal Fourier-transforms of the contestants, by the convolution theorem, which eliminates the integral over time. Thus,

$$\hat{H}_+(\mathbf{r},\, \omega) \;=\; \int_{\mathcal{P}} d^2\mathbf{r}'\; \hat{G}_+(\mathbf{r},\, \mathbf{r}';\, \omega)\hat{\psi}(\mathbf{r}',\, \omega), \tag{10}$$

where $\hat{H}_+$, $\hat{G}_+$ and $\hat{\psi}$ signify the temporal Fourier transforms of H_+, G_+ and ψ, respectively.
As mentioned in the context of Figure 2, it is often useful to render $H_+(\mathbf{r},\, t)$ over a surface, $\mathcal{S}_z$, at a fixed depth, z, beneath $\mathcal{S}_0$. For that purpose, we express the location, $\mathbf{r}$, of the focus by a single depth, z, and the point $\boldsymbol{\rho}$ overlying it on $\mathcal{S}_0$, which we equate to the unit sphere:

$$\mathbf{r} \equiv (\boldsymbol{\rho},\, z). \tag{11}$$

This way, we can regard the derivation of H_+ on $\mathcal{S}_z$ from ψ on $\mathcal{S}_0$, under the specification of appropriate time intervals, regional domains and an appropriate pupil, to be the action of an operator, $P_+(z)$, applied to ψ:

$$H_+(\boldsymbol{\rho},\, z,\, t) = P_+(z)\psi(\boldsymbol{\rho},\, 0,\, t). \tag{12}$$

We call $P_+(z)$ the "(coherent acoustic) regression" operator under the foregoing specifications.

1.4 Subjacent-vantage holography

The diagrams shown in Figures 1 and 2 render the acoustic source as viewed acoustically from above it. This is called "superjacent-vantage" seismic holography. A major complication in solar-interior holography confronted in §1.3 is the acoustic non-uniformity of the solar model, even one that is devoid of local anomalies. The Sun's center is more than 2000 times the temperature of its surface. This is incumbent to a temperature that increases inexorably with depth, z. The sound speed, c, increases with depth accordingly, manifesting strong refraction. Optics in the ray approximation in the solar interior prescribe ray paths, according to Snell's law, whose incidences from vertical inexorably increase with depth. Hence, the solar interior landscape, if there were one, would appear very warped to an acoustic eye that was accustomed to optics in a uniform medium. Indeed, most of the acoustic radiation generated just beneath the surface is refracted back to the surface within a few tens of thousands of km of its source. This adds to the general complication introduced by the optical warpage in an important respect: The major acoustic sources are in essentially the same surface as the pupil—or only barely beneath it. The solar interior more than a few hundred km beneath the surface plays a role in helioseismology only for that component of the acoustic disturbance that propagates downward, penetrating to a significant depth beneath the surface before refracting back to the surface.
An important diagnostic option for this component of acoustic radiation, then, is to focus the computation at the very surface on which it is detected. Holography from this perspective is called "subjacent-vantage" holography. Figure 3 illustrates this application of solar seismic holography in an annular pupil surrounding the surface focus. In the familiar case of

a uniform medium, the ray paths would be straight, and prospective "acoustography" accomplished by a submerged acoustic camera as represented by the lens at the bottom of the Figure. Hence, subjacent-vantage holography of the surface shows the surface in the neighborhood of the focus as it would be seen looking up into it from beneath the surface.
For a rough electromagnetic analogy to subjacent-vantage holography, imagine a photographer using a mirror to photograph an insect on the lens of his camera. This may strike the reader as strange approach to entomology, but, the ability to focus our diagnostic on something we can directly see in electromagnetic radiation offers an exceptionally opportune control resource not to be left begging.

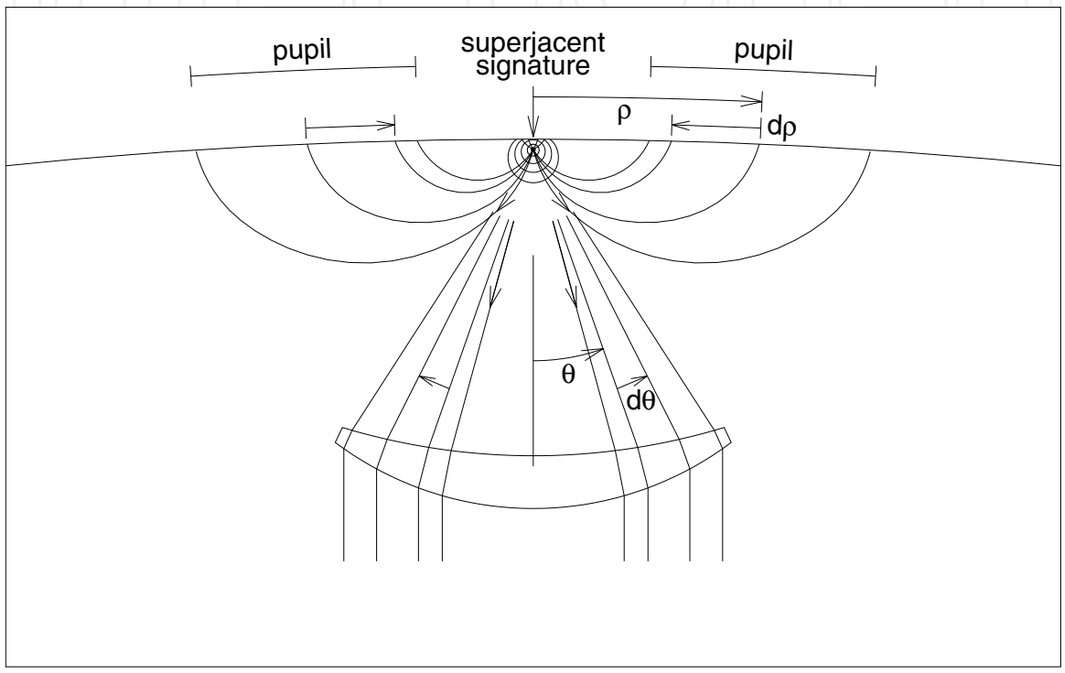

Fig. 3. Subjacent-vantage imaging is the result of a holographic regression in which the focal plane is shallow compared to the inner radius of the pupil. This configuration images seismic radiation that is initially emitted downward from the source and penetrates thousands of km into the solar interior before being refracted back to the surface. While the acoustic disturbance is necessarily observed at the surface, these images render the perspective of an acoustic observer looking upward into the base of the source from thousands of km beneath it. In subjacent-vantage holography, the computational pupil is substantially an inversion of that in familiar lens optics. As the angle, θ, of illumination at the focal point increases, the angular distance, ρ, along the pupil from its center, above the focal point, decreases rather than increases as it does in familiar lens optics.

Comparing the straight ray paths in Figure 3 that apply in a uniform medium with their curved counterparts, it will become apparent that the annular pupil applied in subjacent-vantage holography is somewhat of an inversion of that which applies in lens optics in a uniform medium. The ray directed toward the outer radius of the supposed lens comes to the surface at the inner radius of the annular pupil. Indeed, the diffraction limit of the reconstruction is primarily characteristic of the inner radius, the smaller that being the finer the resolution attained.

Figure 4 shows the result of subjacent-vantage egression-power holography applied to surface observations of a computational simulation of random acoustic disturbances generated just beneath the surface of an acoustic medium that conforms to the solar-interior model of Christensen-Dalsgaard, Proffitt & Thompson (1993). In this simulation, alpha-numeric absorbers, are placed (1) at the surface of the model, and (2) 56 Mm beneath the surface. It will be evident that absorbers play a role in some respects quite the opposite of emitters, casting acoustic silhouettes into the focal planes at their respective depths as opposed to positive signatures.

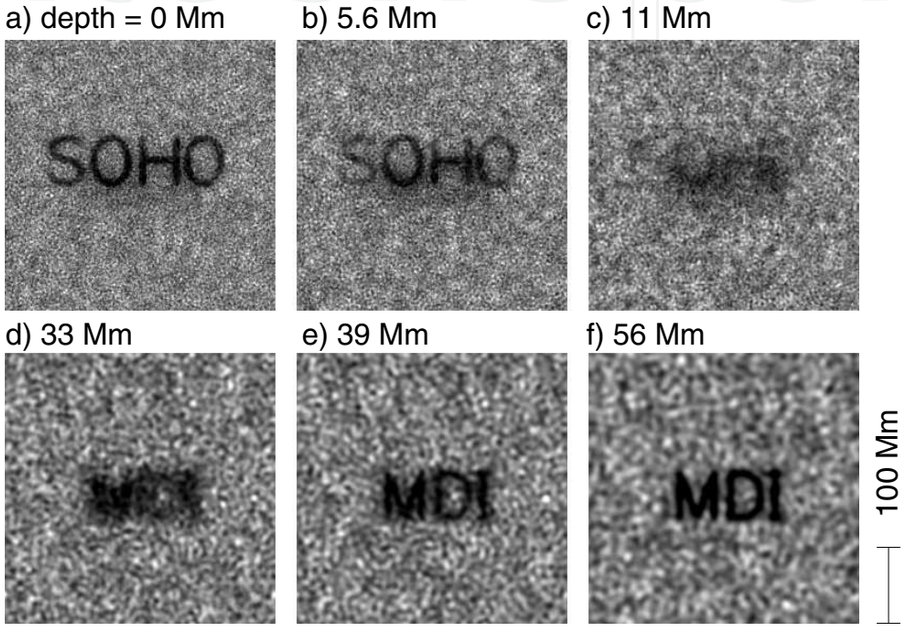

Fig. 4. Egression-power maps of artificial seismic noise that encounters alphanumeric absorbers just beneath the surface and at a depth of 56 Mm. In this simulation, reproduced from Lindsey & Braun (2000b), the absorbers are confined to infinitely thin sheets. Submergence of the focal plane beneath an absorber results not in its disappearance but rather a defocusing of the signature. Diffuse signatures beneath the surface absorbers (frames b and c) and above the submerged absorbers (frames d and e) are a defocus artifact of absorption only at the surface or 56 Mm beneath it and not a signature of additional absorption between those depths.

It is important to observe the distinction between egression-power signatures and the physical properties of the medim that give rise to them. The egression-power signatures of sharp or compact features in egression power maps, for example, may look rather like the source distributions that generate the acoustic waves the signatures represent. However, a diffuse signature may simply represent a source some distance from the focal plane, which itself contains no sources or absorbers whatever. Skartlien (2001) and Skartlien (2002) develop the interesting problem of focus-defocus diagnostics to recover realistic source distributions from egression-power signatures.

2. Helioseismic observations

A wide variety of helioseismic observations have been developed since the advent of helioseismology. The best of these in terms of spatial resolution and stability are from space-borne observatories, the Michelson-Doppler Image (MDI) (Scherrer et al. , 1995) aboard the Solar and Heliospheric Observatory (SOHO), launched by NASA[2] in 1996 and operating into late 2010, and the Helioseismic-Magnetic Imager (HMI) aboard the Solar Dynamics Observatory (SDO), launched early in 2010, also by NASA. The space-borne observatories have been reinforced by observations from a world-wide network of ground-based helioseismic observatories, the Global Oscillations Network Group (GONG), with headquarters at the National Solar Observatory (NSO), in Tucson, Arizona.

During its term of operation, SOHO/MDI made full-disk line-of-sight Doppler maps at a cadence of 60 s with a spatial sampling of $\sim$2 arcsec in its medium-resolution mode of operation, but had a high-resolution, $\sim$0.5 arcsec, mode that covered only part of the solar disk. The SOHO/MDI Dopplergrams were supplemented by occasional intensity and line-of-sight magnetic observations. Since about the turn of the century, the GONG has made full-disk line-of-sight Doppler and magnetic maps and intensity maps, with a resolution of $\sim$2.5 arcsec at a cadence of 60 s.

The SDO/HMI instrument now makes full-disk Doppler, intensity and line-of-sight magnetic maps from a variety of filtergrams at an effective cadence of 45 s with a resolution of $\sim$0.5 arcsec. It also makes Stokes magnetic maps with a cadence of 9 min.

3. Acoustic-power holography of magnetic regions

Figure 5 shows the results of subjacent-vantage acoustic-power holography applied to an actual magnetic region. The upper row shows maps of visible intensity (left) and line-of-sight magnetic field (right) from SOHO/MDI. The middle row shows an acoustic-power map (left) and a subjacent-vantage egression-power map (right) focused at the surface of the region, both in the 5 mHz spectrum (200-s period). The acoustic-power map shows that surface acoustic motion is heavily suppressed in the magnetic regions (Braun et al. , 1992). The egression-power map shows that acoustic radiation emanating downward from the magnetic regions is similarly suppressed.[3] This phenomenon was discovered a decade before the first applications of helioseismic holography by Braun, Duvall & LaBonte (1988) by discriminating ingoing and outgoing wave fluxes in annuli surrounding sunspots. This was a major impetus in the recognition of local helioseismology as a major new field in solar seismology that would include the practical development of helioseismic holography.

Both the acoustic-power maps and the egression-power maps show greater-than-normal power in the peripheries of the active region, where the magnetic field is relatively weak but still greater than it generally is in the quiet Sun. However, the relative distributions of power in "acoustic-power halos" and "acoustic-emission halos" are significantly different. For acoustic radiation with skip distances in the range 15–45 Mm, excess acoustic emission tends to be conspicuous in "magnetic neutral lines", loci along which the magnetic field is approximately horizontal, hence the vertical component of it vanishes (i.e., the line-of-sight component when

[2] National Aeronautics and Space Administration

[3] Because the Doppler signature, ψ, is strongly suppressed in the magnetic region, the power of the raw egression, computed as prescribed by equation (8) is artificially suppressed when the pupil is contaminated by magnetic fields. This suppression is roughly corrected in the middle-right panel by dividing the egression power by a smeared version of the power of the "coherent acoustic *in*gression", a time-reverse analogy of the acoustic *e*gression we will introduce formally in §4.1.

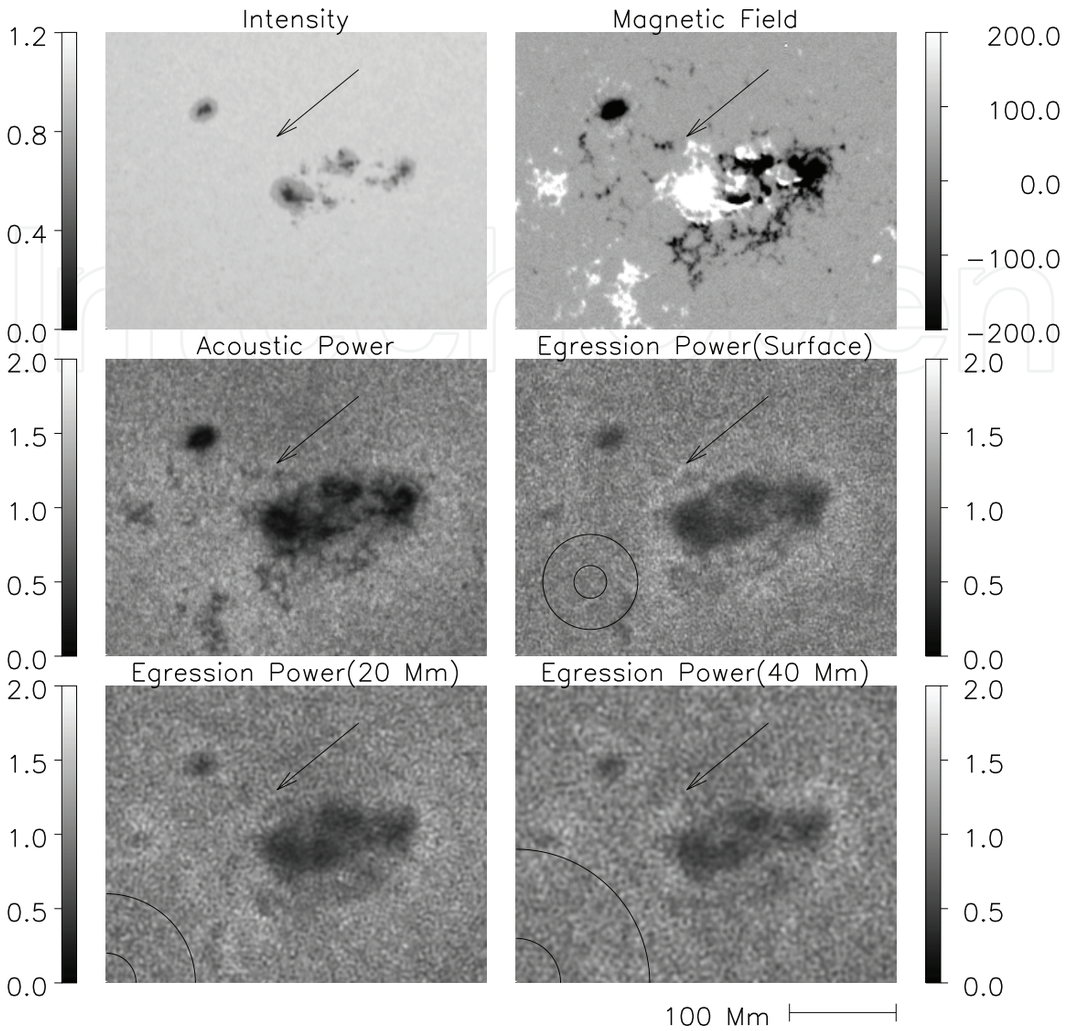

Fig. 5. Egression-power maps of NOAA Active Region 8179. Top panels show intensity (left) and line-of-sight magnetic-field (right) snapshots from SOHO/MDI. Middle-left panel shows a plain 5-mHz acoustic-power map of the region. Middle-right panel shows an egression-power map of the same focused at the surface. The pupil is an annular region with dimensions shown in the lower-left of the panel centered on the focus. Bottom-left panel shows an egression-power map focused at a depth of 20 Mm. Bottom-right panel shows an egression-power map focused at a depth of 40 Mm. An arrow, reproduced in all six frames, points to an excess of seismic emission in the middle-right frame. Acoustic-power and egression-power maps are integrated over a 1 mHz spectrum centered at 5 mHz (i.e., a period of 200 s) and over a duration of 24 hours beginning at 1998 March 15 11:00 UTC.

the active regions is near disk center). An arrow reproduced in all six frames locates such a feature.

The bottom row shows egression-power maps focused 20 and 40 Mm beneath the surface of the active region. The pupils are expanded with increasing depth to keep the vantage subjacent. Because of the increased sound speed, the wavelength of 5-mHz acoustic radiation is greater at greater depths, hence the effects of diffraction are coarser. The main effect of the submerged focal plane appears to be smearing of the egression-power signature.

Interpretation of these signatures is complicated by phase errors now known to be introduced by magnetic fields in the pupils of the acoustic regressions when active regions cannot be entirely avoided (Lindsey & Braun , 2005a). Efforts to account for these phase errors (Lindsey & Braun , 2005a) indicate that surface features such as those seen in Figure 5 are mostly the signature of acoustic anomalies in a relatively thin surface layer. Some investigators (Kosovichev, Duvall & Scherrer , 2000) have suggested the existence of strong acoustic anomalies extending 10 or more Mm beneath sunspot photospheres. The general consensus based on helioseismic holography, however, has been that acoustic anomalies beneath about 2–4 Mm contribute relatively little, perhaps insignificantly, to helioseismic signatures in the neighborhoods of individual active regions.
Because of this, the use of helioseismic holography has developed a strong focus on diagnostics of the relatively shallow subphotospheres of active regions (Lindsey, Cally & Rempel , 2011; Moradi et al. , 2010) as well as the quiet Sun. Results of these studies over the approximately 14 years since the first practical applications of helioseismic holography are considerable, and their descriptions would require more space than we can realistically appropriate in this chapter. Seismic holography of active regions is giving us deep insight into the role of flows in the neighborhoods of active regions (Braun, Birch & Lindsey , 2001), as well the physics of slow- and fast-mode coupling of magneto-acoustic waves in active regions, which seems to be at the heart of how and why active regions suppress acoustic motion in their photospheres and strongly absorb waves that the quiet photosphere normally reflects (Cally , 2000; Cally & Bogdan , 1997; Schunker et al. , 2008; Spruit & Bogdan , 1992). The preponderance of these results involves physics somewhat beyond the familiar scope of optics and holography. We will therefore devote the remainder of this article to two particular phenomena that appear to most easily illustrate the role optics has taken on in helioseismology: (1) acoustic-power holography of transient seismic emission from solar flares, and (2) the use of phase-correlation holography to monitor active regions in the Sun's far hemisphere. Excellent reviews of scientific results from solar acoustic holography in the general context of local helioseismology are contained in Gizon & Birch (2005) and Gizon et al. (2009).

4. Holography of seismic transient emission from flares

4.1 Egression-power signature of a flare

In the solar flare of 1996 July 09, Kosovichev & Zharkova (1998) discovered the first instance of an acoustic transient released into the solar interior by a flare. The surface manifestation of this was a pattern ripples seen in Doppler maps of the active region propagating away from the site of the flare from 15 minutes to an hour after the impulsive phase, what Kosovichev & Zharkova (1998) called a "sunquake". Sunquakes are the surface signature of waves that have traveled tens of thousands of km beneath the foot points of the flare and come back to the surface tens of thousands of km horizontally from the same. Figure 6 shows this phenomenon in a flare in which it was most conspicuous, the X1.2-class flare of 2005 January 15 from NOAA [4] Active Region (AR) 10720. The top row shows intensity (left) and line-of-sight magnetic (right) maps of NOAA AR10720 within an hour before the flare. The middle-left panel shows the Doppler disturbance marking the impulsive phase of the flare, a predominantly red-shifted feature consistent with a downward motion of the photosphere of a few hundred m s^{-1} in a narrow channel aligned along the magnetic neutral line. An arrow, cospatially reproduced in all of the frames, points to the location of this feature. The

[4] National Oceanic and Atmospheric Administration, US Department of Commerce

middle-right panel shows a map of the Doppler signature filtered for temporal variations in a 2-mHz interval centered at 6 mHz 24 minutes after the impulsive phase. A second arrow in this frame points to the most conspicuous surface ripples, 15 Mm above the site of the impulsive disturbance. Nearly cospatial with the impulsive Doppler disturbance shown in the middle-left frame is an impulsive increase in the intensity of a few percent, characteristic of a small white-light flare. This is shown in the lower-left frame.

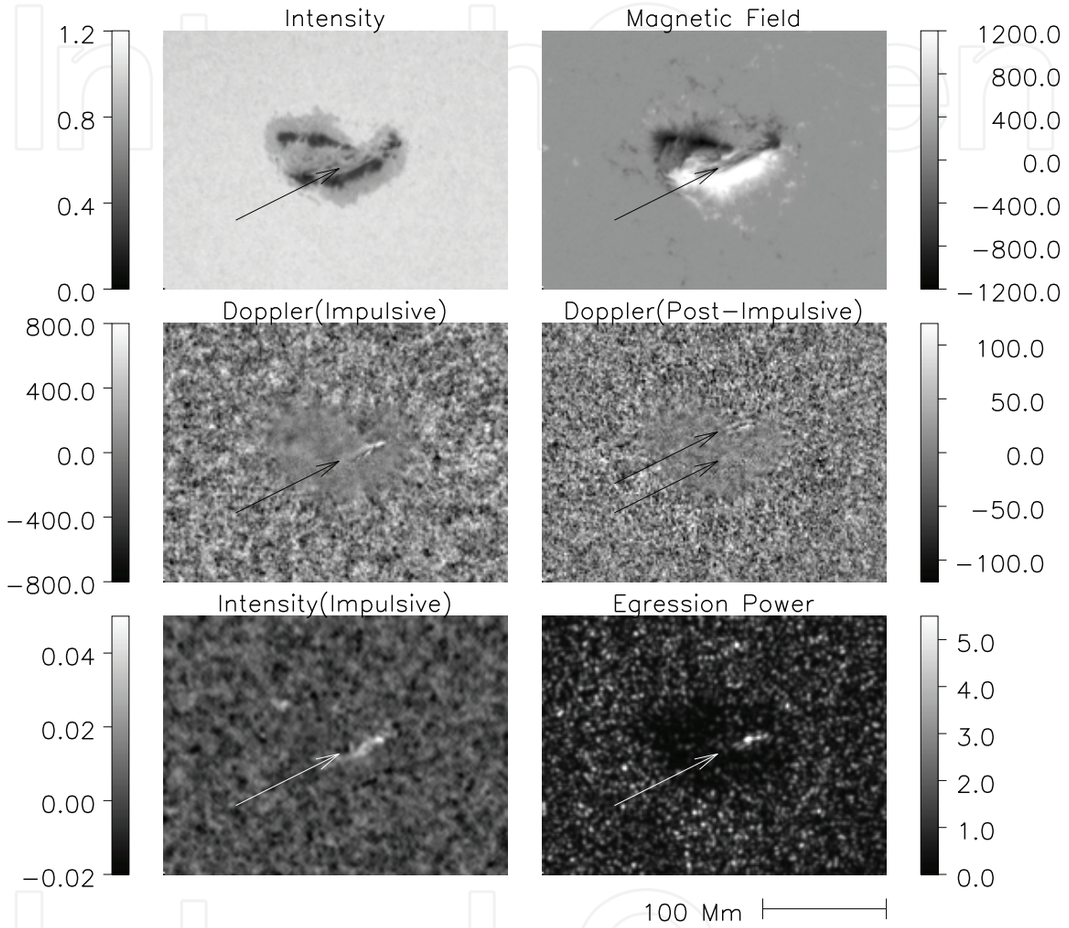

Fig. 6. Helioseismic signature of the X1 flare of 2005 January 15, adapted from Donea (2011). Upper-left panel shows an MDI intensity map of NOAA AR10720 shortly before flare onset. Upper-right panel shows a pre-flare MDI line-of-sight magnetogram of the same. Middle-left panel shows an MDI Doppler map at flare onset, with arrow, reproduced in all other frames, pointing to the sudden, compact red-shift signature at the acoustic source. Middle-right panel shows 6-mHz Doppler signature, ψ, 24 minutes after the onset of the flare. The top arrow in this frame points to surface Doppler ripples proceeding outward from the site located by the lower arrow. Lower-left panel shows the signature of sudden visible continuum emission observed by GONG. Lower-right panel shows an egression-power map of the region during the impulsive phase.

Subjacent-vantage acoustic-power holography of the ripples propagating outward from the site of the impulsive signatures render the source-power distribution of the waves represented by the surface ripples. The lower-right frame shows a map of the 6-mHz egression power

extrapolated subjacently backwards from the post-impulsive ripples to the impulsive phase of the flare. This source pattern is seen to conform closely to the site of both the impulsive intensity and the Doppler transient. In some sunquakes, the acoustic source distribution has coincided with apparent magnetic transients. These diagnostics have motivated models in which seismic transients are thermally driven in some instances, by pressure perturbations associated with impulsive heating (Donea & Lindsey , 2005; Kosovichev & Zharkova , 1998; Lindsey & Donea , 2008; Moradi et al. , 2007), and by Lorentz-force transients in others, due to the sudden release of magnetic free energy (Hudson, Fisher and Welsch , 2008). For a general review, we refer to Donea (2011).

4.2 Discrimination of acoustic radiation from a localized source

In an acoustic medium that conforms to invariance under time reversal, the regression operator, $P_+(z)$, that extrapolates the surface acoustic field backwards in time to a depth z has a counterpart that extrapolates it forward in time. This is accomplished simply by applying the surface disturbance, ψ, represented by surface ripples in Figure 1, to the acoustic model forward in time, as it is observed, rather than in time reverse as illustrated in Figure 2. This computation simply replaces the Green's function, G_+, in equation (8) by its time reverse, G_-, hence,

$$H_-(\mathbf{r},\ t)\ \equiv\ \int_{-\infty}^{\infty} dt' \int_{\mathcal{P}} d^2\mathbf{r}'\ G_-(\mathbf{r},\ \mathbf{r}';\ t\ -\ t')\ \psi(\mathbf{r}',\ t'), \tag{13}$$

where

$$G_-(\mathbf{r},\ \mathbf{r}';\ \tau)\ \equiv\ G_+(\mathbf{r},\ \mathbf{r}';\ -\tau). \tag{14}$$

In the frequency domain,

$$\hat{H}_-(\mathbf{r},\ \omega)\ =\ \int_{\mathcal{P}} d^2\mathbf{r}'\ \hat{G}_-(\mathbf{r},\ \mathbf{r}';\ \omega)\hat{\psi}(\mathbf{r}',\ \omega), \tag{15}$$

and in this context,

$$\hat{G}_-(\mathbf{r},\ \mathbf{r}',\ \omega)\ =\ \hat{G}_+^*(\mathbf{r},\ \mathbf{r}',\ \omega). \tag{16}$$

We call H_-, the counterpart of the coherent acoustic egression, the "(coherent acoustic) *in*gression", and the operator, $P_-(z)$, that derives it from ψ the "(coherent acoustic) *pro*gression" operator, whereby equation (12) generalizes to,

$$H_\pm(\mathbf{r},\ z,\ t)\ =\ P_\pm(z)\psi(\mathbf{r},\ 0,\ t). \tag{17}$$

For a lossless medium that conforms to time-reversal invariance, and in the limit of a pupil, $\mathcal{P}$, with an infinitesimal inner radius that otherwise covers the entire solar surface, the successive application of $P_-(0)$ and $P_+(0)$ returns ψ itself:

$$P_-(0)P_+(0)\psi(\mathbf{r},\ 0,\ t)\ =\ \psi(\mathbf{r},\ 0,\ t), \tag{18}$$

so long as ψ represents acoustic waves that propagate downward some distance from the surface into the solar interior before they are turned back to the Sun's surface. This, along with the spatial discrimination the regression gives us with respect to waves emitted from the source region, makes it possible to isolate the component of acoustic radiation emanating from just the source region. Figure 7 demonstrates this exercise applied to the flare of 2005 January 15. The top two frames show the 6-mHz Doppler disturbances, ψ, during the impulsive phase (left) and 24 minutes after (right). Having applied $P_+(0)$ to ψ we examine the distribution in egression-power, $|H_+(\mathbf{r},t)|^2$, during the impulsive phase and outline the source region of interest. This is rendered by the parameceoid inset of the egression-power distribution in the

middle-right frame of Figure 7. We then apply a spatial mask, M, admitting only this part of $H_+(\mathbf{r},\ t)$, and finally apply $P_-(0)$ to the masked egression to reverse the regression. The full operation, then, is

$$\psi_M(\mathbf{r},\ 0,\ t)\ =\ P_-(0)MP_+(0)\psi(\mathbf{r},\ 0,\ t). \tag{19}$$

The result, ψ_M, 24 minutes after the impulsive phase is rendered in the middle-right frame of Figure 7 surrounding of the egression-power inset. The acoustic power, $|\psi_M(\mathbf{r},t)|^2$, from the source region is rendered directly below, in the lower-right frame. The lower-left frame plots the power at this moment along a circle of radius 22.4 Mm, drawn in the lower-right frame. The non-uniform directional distribution of the acoustic radiation is the signature of a source that is not only spatially extended, as is evident from the egression-power map, but one that is undergoing complex motion (Donea & Lindsey , 2005; Kosovichev , 2007).
These diagnostics offer considerable promise towards an understanding of the nature of the impetus that drives transient seismic emission into the solar interior.

5. Seismic signatures of active regions in the Sun's far hemisphere

Time-distance statistics by Duvall et al. (1993) showed that acoustic radiation in the 2.5–4.5 mHz band propagates from the near hemisphere to the far hemisphere and back, retaining significant coherence. It might seem, then, that seismic imaging of the Sun's far hemisphere would be simply a matter of extending the pupil, $\mathcal{P}$, of a holographic regression to the hemisphere opposite to the focus. The understanding here is that the pupil is in the hemisphere accessible to observations of the acoustic field, ψ; hence, the focus is in the far hemisphere. It turns out that the preponderance of acoustic radiation that survives the trip from one hemisphere to the other does so by benefit of at least one specular reflection from the surface.[5] But, these species of acoustic radiation, those which penetrate deep into the Sun's interior and skip long distances, appear to be rather poorly absorbed by most of the magnetic region. For these waves, magnetic regions act more as scatterers than absorbers. Because of this, seismic monitoring of the Sun's far hemisphere is based heavily on two basic elements:

1. phase-correlation seismology, and
2. the extension thereof to multiple-skip acoustics.

5.1 Phase-correlation holography

Acoustic-power holography is highly effective for detecting and locating local absorbers or emitters in an environment in which these are prevalent. However, it is not generally very effective for detecting elastic scatterers in a non-absorbing acoustic medium bounded by a specularly reflecting surface. A scatterer does indeed block radiation that would otherwise have registered at the focus of a holographic computation, casting a silhouette with respect to it in technical terms. However, in a nominally isotropic radiative environment, the scatterer generally replaces the radiation it blocks with radiation that would have missed the focus, filling the silhouette with radiation as bright as that which was blocked. The imposition upon efforts to detect a scatterer based on egression power, then, is rather like that upon having to see white cat in a white room.[6] It is rather the character of an efficient scatterer to shift the *phase* of radiation that encounters it than its intensity.

[5] Duvall et al. (1993) found that the Sun's surface becomes a strong absorber of acoustic radiation much above 4.5 mHz in frequency, a result Lindsey & Braun (1999) confirmed by 2-skip seismic holography (see also Braun & Lindsey , 2000a).

[6] We thank former NSO summer student Mark Fagan for this metaphor.

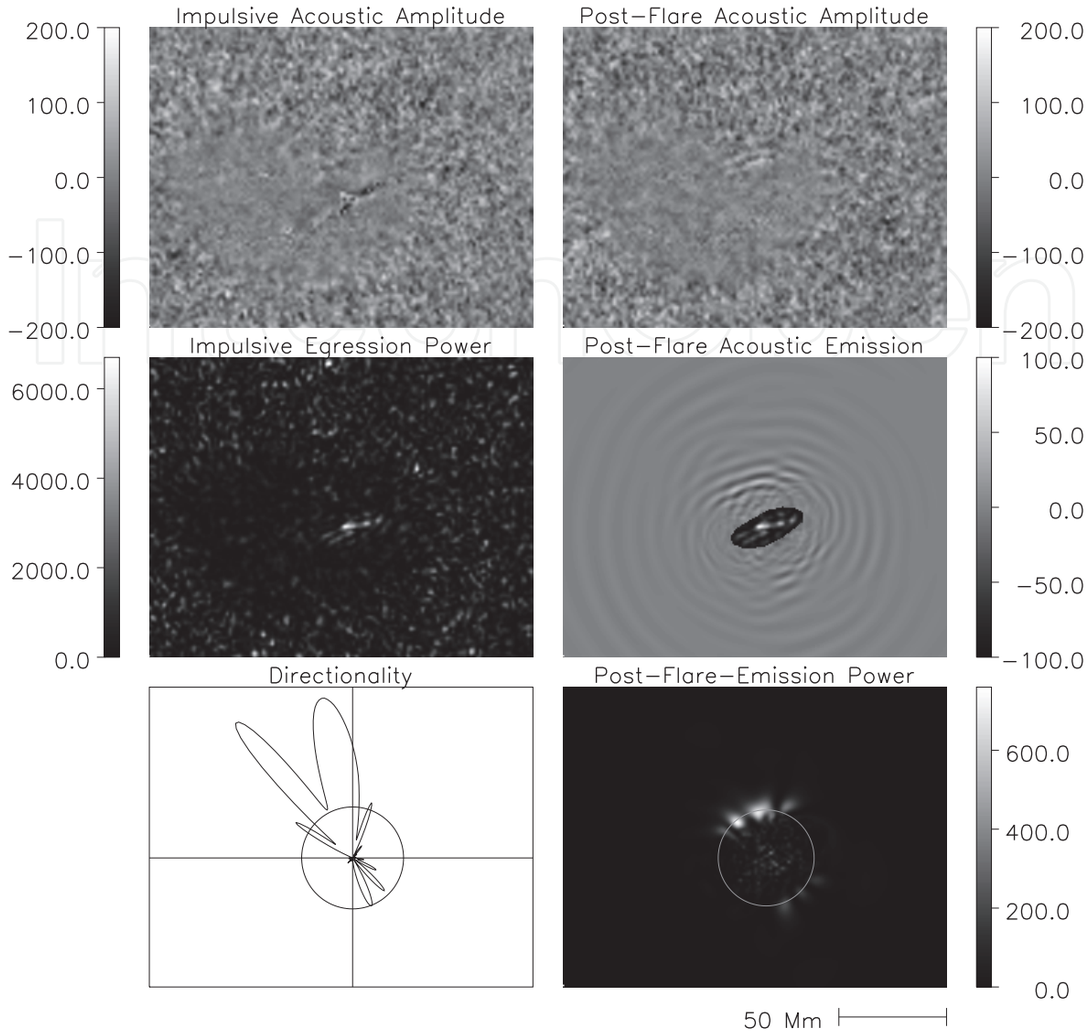

Fig. 7. Discrimination of the component of the 6-mHz Doppler signature, ψ, emanating from the site of transient emission shown in Figure 6, adapted from Donea (2011). Upper-left panel shows the 6-mHz Doppler signature, ψ, at flare onset. Upper-right panel shows the same 24 minutes after flare onset. Middle-left panel shows the 6-mHz egression power at flare onset. Middle-right panel shows a holographic representation of the component, ψ_M, of ψ that has emanated from the source region, marked by the inset of the egression power from the source region, 24 min after flare onset. Lower-right panel shows the acoustic power, $|\psi_M|^2$, emanating from the source region 24 min after flare onset. Lower-left panel plots the acoustic power, $|\psi_M|^2$, along the 22.4-Mm-radius circle in the lower-right frame. The circle plotted in the lower-left frame represents an egression power of 200 m^2 s^{-2}.

Figure 8 shows 5-mHz phase maps of cospatial correlations between H_+, H_-, focused subjacently at the Sun's surface from the near hemisphere, and with ψ, in the neighborhood of NOAA AR8179. H_+ and H_- are computed here over the same pupil as applied in the middle right frame of Figure 5. Top two frames show intensity (left) and line-of-sight magnetic field (right). Middle left frame shows normalized egression-power, $\langle |H_+(\mathbf{r},t)|^2 \rangle$, reproduced from Figure 5; and the arguments of $\langle H_+ H_-^* \rangle$ (middle-right); $\langle H_+ \psi^* \rangle$ (lower-left);

and $\langle \psi H_-^* \rangle$ (lower-right). We call the correlations of $H_\pm$ with ψ (bottom row) the "control correlations", since they compare extrapolations of ψ from the pupil with ψ itself. The "ingression control correlation" phase, $\arg \langle \psi H_-^* \rangle$, in an active region expresses how the active region shifts the phases of the acoustic signatures of waves impinging into it from beneath the photosphere. The egression-ingression correlation $\langle H_+ H_-^* \rangle$ characterizes how the active region reflects these same waves back into the Sun's interior. The negative deflection in its phase, $\arg \langle H_+ H_-^* \rangle$, for foci in the active region is the signature of reflected waves that arrive into the egression pupil up to $\sim$100 s ahead of their counterparts reflecting from the quiet solar surface. In recent models of sunspots, these reduced travel times appear to be largely the result of something like a $\sim$300 km depression in the photospheres of sunspot umbrae (Lindsey, Cally & Rempel , 2011). This interpretation is a great oversimplification of the reality. However, because it works very well as a model, we have characterized this seismic quality of active regions as an "acoustic Wilson depression", bearing in mind a likely relationship to the well-known Wilson effect discovered by Alexander Wilson in the 16$^{\text{th}}$ century. In the case of the signatures shown in Figure 8, the phase shifts tend to be enhanced in sunspot penumbrae, where the magnetic field is highly inclined. However, these effects extend far outside of the sunspots into regions in which the magnetic field is less than 1 kG. Because of this, the integrated seismic signature of the active region is several times that due to the sunspots alone. This greatly enhances the acoustic visibility of a large active region in the Sun's far hemisphere. And, unlike in the case of absorption, the phases of waves that skip long distances are roughly as sensitive sensitive to the acoustic Wilson depression as those whose phase perturbations are mapped in Figure 8.

5.2 Multiple-skip holography

Because the sound speed in the solar interior increases by such a large factor from the surface to the Sun's core, only a small fraction of the acoustic radiation generated at the surface penetrates deep beneath the Sun's surface before coming back to the surface. The ray paths that connect a point at the center of the far hemisphere to a pupil in the near hemisphere whose radius is 0.9 times the radius of the solar disk must emanate downward within a vertical cone whose half-angle, α, is 0.22°, a rapidly decaying quasi-exponential function of the skip distance. The resulting diffraction limit,

$$w \;=\; cT/\sin\alpha, \tag{20}$$

—where $c = 8$ km s^{-1} is the photospheric sound speed and $T \sim 300$ s, is the wave period—is prohibitive: For a conical half-angle, α, of 0.22°, w is 630 Mm, nearly a solar radius and much larger than the largest active regions, even including their plages.

Fortunately, waves with periods of $\sim$300 s incident into the Sun's surface from beneath it are known to be largely reflected back into the solar interior Duvall et al. (1993). The reflection is of good specular quality, such that coherence is significantly preserved over a several skips beneath the Sun's surface (Lindsey & Braun , 1999). It is straight-forward to formulate the Green's functions, $G_\pm$, to account for this, making multiple-skip holography practical. Ray paths that cover the same distance in two skips, by reflecting once from the solar surface subtend a cone that is much wider (i.e., not nearly as decayed), by a factor of a factor of about five, to 1.2°. The extra skip, then, greatly improves the diffraction limit, w, to $\sim$120 Mm, the scale of a moderately large active region.

Figure 9 shows a diagram of ray paths and matching wave-front geometries representing the basic acoustical elements of 2×2-skip phase-correlation holography of the Sun's far hemisphere (top) from the vantage of the near hemisphere (bottom), as derived by the far-side

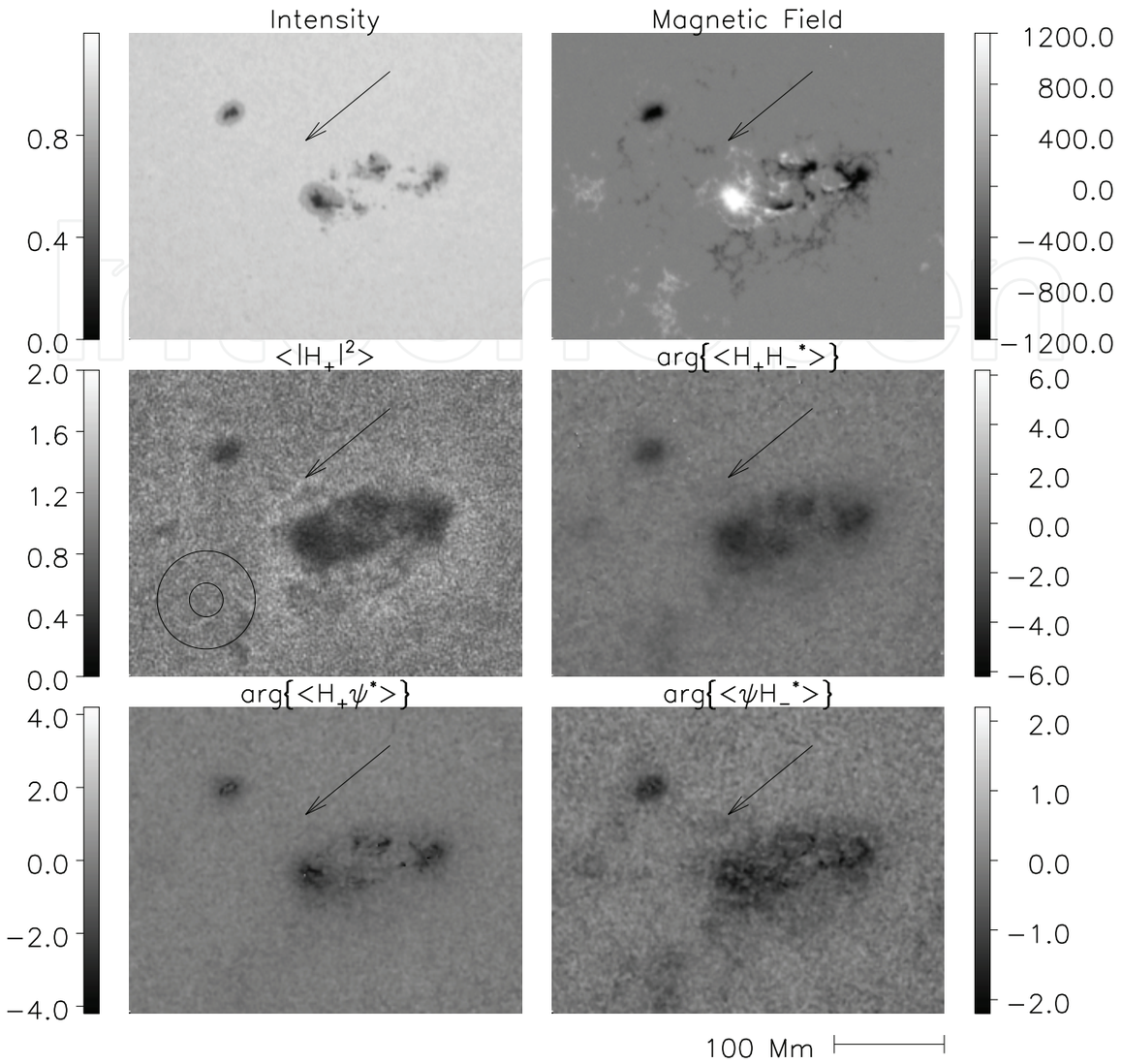

Fig. 8. Phase maps of correlations between 5-mHz $H_{\pm}$ and ψ. Upper row shows intensity and line-of-sight-magnetic maps of AR8179, reproduced from Figure 5. Middle-left panel renders 5-mHz egression power reproduced from Figure 5. Middle-right panel shows the egression-ingression correlation phase, $\arg\{\langle H_+ H_-^* \rangle\}$ in radians. Bottom-left panel shows the egression control correlation phase, $\arg\{\langle H_+ \psi^* \rangle\}$. Bottom-right panel shows the ingression control correlation phase, $\arg\{\langle \psi H_-^* \rangle\}$. The arrow, cospatially placed in all frames points to the narrow channel of enhanced 5-mHz emission in the egression-power map (middle-left frame).

seismic synoptic monitors presently operating at the headquarters of the NSO/GONG project, in Tucson, and the Joint Science Operations Center of the SDO, at Stanford University. The acoustic travel times along the trajectories plotted in Figure 9 are approximately 3.5 hours from the near hemisphere to the focus in the far hemisphere. The round trip travel time, then, for a disturbance in the near hemisphere to its echo in the near hemisphere from the focus is about 7 hours. To detect the phase correlation between H_+ and H_-, then, requires

observations of the near hemisphere for at least this period before correlation statistics can begin to accumulate.

The first far-side seismic maps, based on 2×2-skip acoustics were published by Lindsey & Braun (2000a), computed from helioseismic observations by SOHO/MDI. The Solar Oscillations Investigation (SOI) at Stanford University implemented a synoptic far-side seismic monitor using the 2×2-skip algorithm in early 2001, which continued to operate until the recent expiration of SOHO/MDI in early 2011.

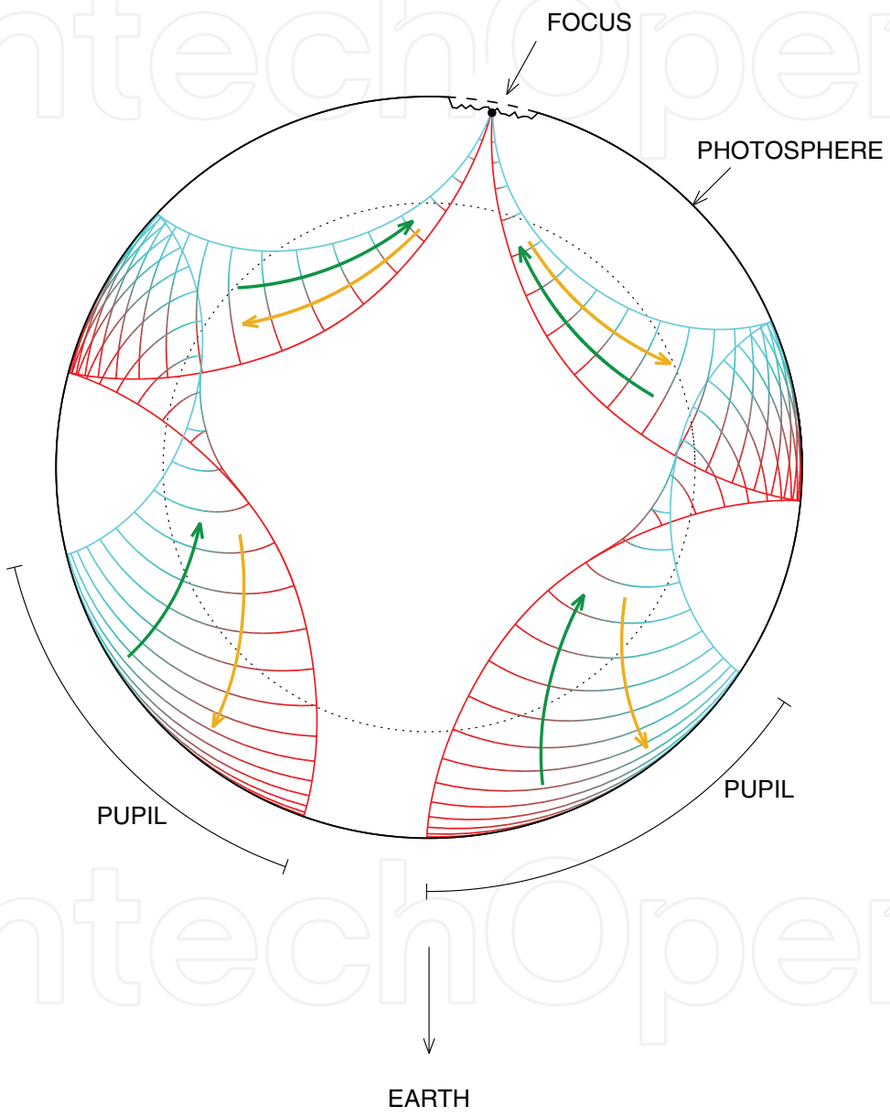

Fig. 9. Diagram of ray paths and matching wave-front geometries representing 2×2-skip phase-correlation holography of the far (top) hemisphere of the Sun from observations over a pupil in the near (bottom) hemisphere.

The 2×2-skip algorithm is only sensitive to active regions within ∼50° of the antipode of disk center in the near hemisphere. Braun & Lindsey (2001) extended the algorithm to cover the full far hemisphere by incorporating 1×3-skip acoustics. Both the GONG and the SDO now have synoptic far-side seismic monitors covering the full far hemisphere of the Sun.

Figure 10 shows maps of the phase of $\langle H_+ H_-^* \rangle$ of the far hemisphere computed from GONG observations, using the foregoing schemes to cover the full far hemisphere. In this presentation, the "Carrington" mapping, the Sun's surface is rendered by longitude and latitude in a co-rotating reference frame in which active regions are nearly stationary. Hence, it is the region viewable from Earth that moves, from right to left as the Sun rotates from east (left) to west (right) with respect to Earth. Each map represents a compilation of statistics from observations over a 24-hour period, effectively 17 hours when an account is taken of the 7-hr round-trip travel time. The signature of what was to be designated NOAA AR10808 is seen passing across the far eastern hemisphere from Earth perspective, rotating into direct view a week after crossing far-side central meridian. Upon its arrival at the eastern limb, this active region released an X17-class flare, one of the most intense in recorded history—and one of the best observed, largely because of preparations motivated by expectations based on the holographic signatures. For a deeper discussion relating holographic phase-correlation signatures in the far hemisphere to magnetic and other signatures as directly viewed in the near hemisphere, we refer to González Hernández, Hill & Lindsey (2007).

The ability to monitor activity in the Sun's far hemisphere has become a major asset in space-weather forecasting (González Hernández et al. , 2009), including solar-irradiance forecasting (Fontenla, et al. , 2009). UV solar irradiance has a strong effect the terrestrial ionosphere and exosphere, which determines the rates at which the orbits of spacecraft and space debris decay. Improved forecasting of solar UV irradiance is therefore a major object of agencies whose task is to keep track of a large inventory of orbiting debris from ground-based observations that can be interrupted by poor weather.

It also occasionally happens that a flare or coronal mass ejection (CME) emanating from the Sun's far hemisphere has a significant effect on the near-Earth environment. An example of this was the halo CME of 2001 August 15–16. The upper-right panel of Figure 11 shows an image of the CME in the Large Angle Spectrometric Coronagraph (LASCO) aboard SOHO at the outset of its progression into the interplanetary medium. The lower-right panel shows the 2×2-skip phase-correlation map from Earth perspective, the signature of a newly born active region appearing below and somewhat to the left of far-side disk center, having crossed far-side central meridian about a day before. NOAA designated this AR09591 a few days after it rotated into direct view from Earth. The lack of significant X-ray emission from this event (lower-left panel) is simply a result of its having occurred in the far hemisphere. I.e., copious X-rays must certainly have been released by such an event, but these would have been radiated into the far side of the solar system, hence invisible from Earth. This does not apply to high-energy charged particles, which are strongly deflected by magnetic fields that are probably involved in their acceleration, possibly a considerable distance from the location of the active region as indicated by its helioseismic signature. As the upper-left panel of Figure 11 shows, a considerable flux of high-energy protons showered the near-Earth environment promptly following the appearance of this CME. In this instance, this happened to be of significant concern to crew members of the International Space Station (ISS), who were undertaking an extra-vehicular activity (EVA) at the time.

Events such as that shown in Figure 11 happen rarely, perhaps only once in an 11-year solar-activity cycle, and helioseismic signatures of active regions in the far hemisphere cannot give us a very reliable assessment of the potential of an active region in the far hemisphere breaking all rules of fairness and decency to impose upon the near-Earth environment this way. Indeed, we do not yet have this capability even for an active region in direct view, in which case the particle flux to be expected is many times greater, posing a significant health hazard to an exposed crew. The ability to monitor large active regions in the Sun's far hemisphere nevertheless greatly facilitates planning of activities to which flares pose a

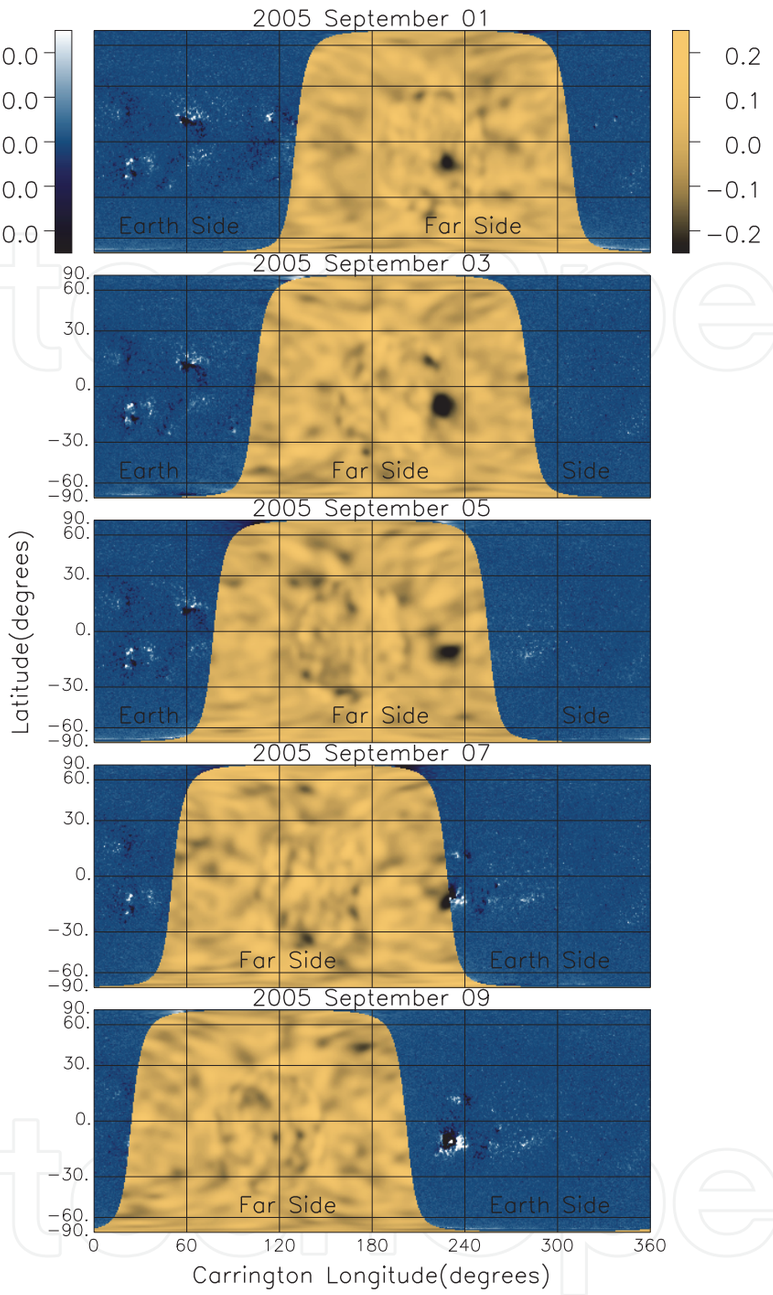

Fig. 10. The phase of $\langle H_+ H_-^* \rangle$ focused on the surface of the Sun's far hemisphere is compared with line-of-sight magnetic maps in the near hemisphere as viewed directly from earth over the period 2005 September 01–09. The signature of NOAA AR10808 is seen just after crossing far-side central meridian on September 01, the region rotating into direct view from Earth on September 07.

considerable liability, particularly on time scales of a week or two when the existences of active regions that could produce them have yet to be announced by any other means.
Since its implementation in the early 2000s, the helioseismic monitor of the Sun's far hemisphere has been complemented by measurements of Ly-α radiation back-scattered from

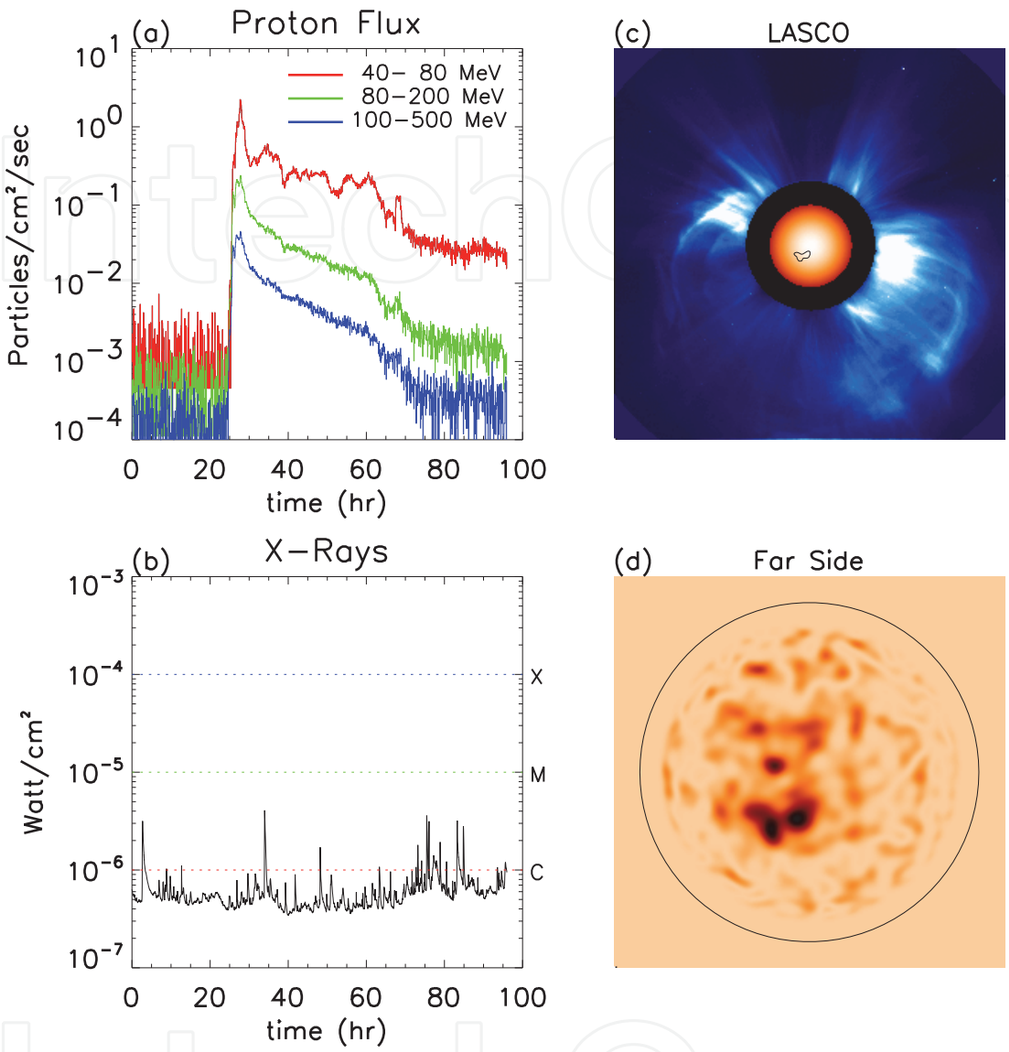

Fig. 11. High-energy-proton and X-ray fluxes associated with a large far-side CME occurring on 2001 August 15–16 . Panel *a* shows plots of the proton flux detected by the GOES–10 spacecraft at energies ranging from 40 to 500 MeV in 96-hr period beginning at 2001 August 15, 00:00 UT. Panel *b* shows plots of the 1–8Å X-ray flux in the same time frame. Panel *c* shows a LASCO image of the CME at August 16, 00:31 UT, approximately one hour after first evidence of the CME in the LASCO coronagraphs. The Sun's surface is represented by a solar icon at the center of the LASCO image. A closed contour drawn on the solar icon represents the location of active regions in the Sun's far hemisphere that were to be designated 9557 and 9591 a few days later when they rotated into direct view. Panel *d* shows a far-hemisphere map of arg $\langle H_+ H_-^* \rangle$ as viewed from LASCO perspective through the near hemisphere and intervening solar interior. The composite signature of the two active regions is seen approximately 0.3 solar radii south (below) and slightly east (left) of far-side disk center.

the interplanetary medium in the far side of the solar system, the major component of which originates from active regions in the Sun's far hemisphere (Fontenla, et al. , 2009; Quemerais & Bertaux , 2006). The instrument that makes these measurements is the Solar Wind ANisotropies (SWAN) experiment, on SOHO.
As of early 2011, NASA's two STEREO spacecraft have had full coverage the Sun's far-hemispheric corona with X-ray observations. The STEREO spacecraft will continue to enjoy this full far-hemispheric coverage until about 2019.

6. The future of helioseismic holography

Helioseismic holography will certainly continue to play a major role in helioseismology, and in solar research at large, for the foreseeable future. Nearly all of the applications to date have focused on relatively compact anomalies near the Sun's surface. This is largely because these manifest the strongest and most compact signatures, the ability of which to discriminate spatially is the significant advantage of the optical perspective. And, in certain respects, these superficial features play the role of an "acoustic showerglass" we have to look through to see what lies beneath them (Lindsey & Braun , 2005a;b). However, the availability of ever more powerful computing facilities encourages the extension of seismic holography deep into the solar convection zone. This offers the possibility of new insight into the workings of the solar dynamo, the origin of emerging solar activity.
The prospect of seismic holography of the deep solar interior is further encouraged by plans under development by NASA and ESA[7] to include helioseismometers on spacecraft in heliocentric orbits with direct vantages into the Sun's far hemisphere. Simultaneous seismology of both hemispheres offers the best prospects for rotational diagnostics of the Sun's core, which maintains the nuclear reactions that have kept the Sun alive for eons.
The application of seismic holography to more than a hundred emerging active regions during solar cycle 23 (Birch et al., 2009) shows tantalizing signatures up to three days before the significant emergence. These signatures are not strong enough to forecast active-region emergences on an individual basis. However, the statistical existence of these signatures has major implications respecting the dynamics of magnetic flux approaching the Sun's surface from below. This entails the tantalizing suggestion that such a forecast will be possible once we understand the dynamics underlying the pre-emergence signatures.
In summary, then, this book adds to a wide consensus that optics must certainly be one of the extremely few most powerful diagnostic tools nature has given us. The extension of electromagnetic optics to other wave-mechanical resources has already been a very welcome development such as in electron microscopy, acoustic microscopy, under-water acoustics and geoseismology. It is now beginning to render major benefits in our understanding of the interior workings of the star we live by. Helioseismic holography is a young and growing field of scientific research. We are convinced it will lead to many satisfying benefits in the coming generation.

7. Acknowledgments

We dedicate this chapter to the memory of solar physicist Karen Lorraine Harvey (1942–2002). Many people have contributed to the technical development of solar acoustic holography since it was first proposed, 35 years ago, especially in the past 20 years. We are especially grateful for the unflagging support of Jack Harvey, at the National Solar Observatory, and his late wife, Karen, who supported this work with the resources of the Solar Physics

[7] European Space Agency

Research Corporation. We thank Aaron Birch for his consultation. The development of helioseismic holography has received invaluable support from the Solar-Terrestrial and Astronomy-and-Stellar-Astrophysics Branches of the National Science Foundation and from the National Aeronautics and Space Administration during the past two decades.

8. References

Birch, A. C. & Braun, D. C.; Leka, K. D.; Barnes, G.; Dunn, T. L. & González Hernández, I. (2009). A Search for pre-emergence signatures of active regions. *Bul. Am. Astronom. Soc., Sol. Phys. Div.*, Vol 41, 810

Born, M. & Wolf, E. (1975a). *Principles of Optics*, 491–505, Pergamon Press, Oxford

Born, M. & Wolf, E. (1975b). *Ibid.*, 375–378

Braun, D. C.; Duvall, T. J. Jr. & LaBonte, B. J. (1988). The absorption of high-degree p-mode oscillations in and around sunspots. *Astrophys. J.*, Vol. 335, 1015–1025

Braun, D. C.; Lindsey, C.; Fan, Y. & Jefferies, S. M. (1992). Local acoustic diagnostics of the solar interior. *Astrophys. J.*, Vol. 392, 739–745

Braun, D. C., Lindsey, C., Fan, Y. & Fagan, M. (1998). Helioseismic holography of solar activity. *Astrophys. J.*, Vol. 502, 968–980

Braun, D. C. & Lindsey, C. (2000a). Helioseismic holography of active-region subphotospheres. *Solar Phys.*, Vol. 192, 285–305

Braun, D. C. & Lindsey, C. (2000b). Phase-sensitive holography of solar activity. *Solar Phys.*, Vol. 192, 307–319

Braun, D. C. & Lindsey, C. (2001). Seismic imaging of the far hemisphere of the Sun. *Astrophys. J. Letters*, Vol. 560, 189–192

Braun, D. C.; Birch, A. C. & Lindsey, C. (2004). Local helioseismology of near-surface flows. *Helio- and Asteroseismology: Towards a Golden Future. Proceedings of the SOHO 14/GONG 2004 Workshop*, E. Danesy (Ed.), (ESA SP559) pp. 337–340, ESA, Yale University, New Haven

Christensen-Dalsgaard, J.; Proffitt, C. R. & Thompson, M. J. (1993). A new technique for measuring solar rotation. *Astrophys. J. Letters*, Vol. 403, 75–78

Cally, P. S. (2000). Modelling p-mode interaction with a spreading sunspot field. *Solar Phys.*, Vol. 192, 395–401

Cally, P. S. & Bogdan, T. J. (1997). Simulation of f- and p-mode interactions with a stratified magnetic field concentration. *Astrophys. J. Letters*, Vol. 486, 67–70

Chang, H.-K., Chou, D.-Y., LaBonte, B. J. & the TON Team (1997). Ambient acoustic imaging in helioseismology. *Nature*, Vol. 389, 825–827

Chou, D.-Y. (2000). Acoustic imaging of solar active regions. *Solar Phys.*, Vol. 192, 241–259

van Cittert, P. H. (1939). Kohärenz probleme. *Physica*, Vol. 6, 1129–1138

Claerbout, J. F. (1997). *Imaging the Earth's Interior* Nikos Dracos, Computer Based Learing Unit, University of Leeds

Deubner, F.-L. (1975). Observations of low wavenumber nonradial eigenmodes of the Sun. *Astron. & Astrophys*, Vol. 44, 371–375

Donea, A.-C. (2011). Seismic transients from flares in solar cycle 23. *Space Science Reviews* in press

Donea, A.-C.; Braun, D. C. & Lindsey, C. (1999). Seismic images of a solar flare. *Astrophys. J. Letters*, Vol. 513, 143–146

Donea, A.-C. & Lindsey, C. (2005). Seismic emission from the solar flares of 2003 October 28 and 29. *Astrophys. J.*, Vol. 630, 1168–1183

Donea, A.-C.; Lindsey, C. & Braun (2000a). Stochastic seismic emission from acoustic glories and the quiet Sun. *Solar Phys.*, Vol. 192, 321–333

Duvall, T. L. Jr.; Jefferies, S. M.; Harvey, J. W. & Pomerantz, M. (1993). Time-distance helioseismology. *Nature*, Vol. 362, 430–432

Duvall, T. L. Jr.; D'Silva, S.; Jefferies, S. M.; Harvey, J. W. & Schou, J. (1992). Downflows under sunspots detected by helioseismic tomography. *Nature*, Vol. 379, 235–237

Evans, J. W.; Michard, R.; Servajean, R. (1963). Observational Study of macroscopic inhomogeneities in the solar atmosphere. V. Statistical Study of the time variations of solar inhomogeneities. *Astron. & Astrophys.*, Vol. 26, 368–382

Fontenla, J. M.; González Hernández, I.; Quémerais, E. & Lindsey, C. (2009). Solar irradiance forecast and far-side imaging. *Adv. in Space Sci.*, Vol. 44, 457–464

Gizon, L. & Birch, A. C. (2005). Local Helioseismology. In *Living Reviews in Solar Physics*, S. Solanki, J. Christensen-Dalsgaard, B. Foleck, E. Marsch, R. Rosner, T. Sakurai, K. Schrijver, M. Schüssler & R. Schwenn (Eds.), Vol. 2, Max Planck Gesellschaft, `http://solarphysics.livingreviews.org`

Gizon, L., Schunker, H., Baldner, C. S., Basu, S; Birch, A. C.; Bogart, R. S.; Braun, D. C.; Cameron, R.; Duvall, T. L.; Hanasoge, S. M.; Jackiewicz, J.; Roth, M.; Stahn, T.; Thompson, M. J. & Zharkov, S. (2009). Helioseismology of sunspots: A case study of NOAA Region 9787. *Space Science Reviews*, Vol. 144, 249–273

González Hernández, I.; Hill, F. & Lindsey, C. (2007). Calibration of the far sid seismic-holography signature of active regions. *Astrophys. J.*, Vol. 669, 1382–1389

González Hernández, I.; Hill, F.; Scherrer, P. H.; Lindsey, C. & Braun, D. C. (2009). On the success rate of the farside seismic imaging of active regions. *Space Weather* Vol. 8, S06002

Hudson, H.S.; Fisher, G. H. & Welsch, B. T. (2008). Flare energy and magnetic field variations. *Subsurface and Atmospheric Influences on Solar Activity, ASP Conf. Series* Vol. 383, R. Howe, R. Komm, K. S. Balasubramaniam & G. J. D. Petrie (Eds.), pp. 221–226, National Solar Observatory, Sunspot, NM, 16–20 April 2007, Astronomical Society of the Pacific

Kosovichev (2007). The cause of photospheric and helioseismic responses to solar flares: High-energy electrons or protons. *Astrophys. J. Letters*, Vol. 670, 65–68

Kosovichev, A. G.; Duvall, T. L. Jr. & Scherrer, P. H. (2000). Time-distance inversion methods and results. *Solar Phys.*, Vol 192, 159–176

Kosovichev, A. G. & Zharkova, V. V. (1998). X-ray flare sparks quake inside Sun. *Nature*, Vol 393, 317–318

Leighton, R. B.; Noyes, R.; Simon, G. (1962). Velocity fields in the solar atmosphere. Preliminary report. *Astrophys. J.*, Vol. 135, 474–499

Lindsey, C. & Braun, D. C. (1990). Helioseismic imaging of sunspots at their antipodes. *Solar Phys*, Vol. 135, 474–499

Lindsey, C. & Braun, D. C. (1997). Helioseismic Holography. *Astrophys. J.*, Vol. 485, 895–903

Lindsey, C. & Braun, D. C. (1999). Chromatic holography of the sunspot acoustic environment. *Astrophys. J.*, Vol. 510, 494–504

Lindsey, C. & Braun, D. C. (2000a). Seismic Images of the Far Side of the Sun. *Science*, Vol. 287, 1799–1800

Lindsey, C. & Braun, D. C. (2000b). Basic Principles of Solar Acoustic Holography. *Solar Phys.*, Vol. 192, 261–284

Lindsey, C. & Braun, D. C. (2005a). The acoustic showerglass. I. Seismic diagnostics of photospheric magnetic fields. *Astrophys. J.*, Vol. 620, 1107–1117

Lindsey, C. & Braun, D. C. (2005b). The acoustic showerglass. II. Imaging active-region subphotospheres. *Astrophys. J.*, Vol. 620, 1118–1131

Lindsey, C.; Cally, P. S. & Rempel, M. (2010). Seismic discrimination of thermal and magnetic anomalies in sunspot umbrae. *Astrophys. J.*, Vol. 719, 1144–1156

Lindsey, C. & Donea, A.-C. (2008). Mechanics of seismic emission from flares. *Solar Phys.*, Vol. 651, 227–639

Lindsey, C.; Braun, D. C.; Jefferies, S. M.; Woodard, M. F.; Fan, Y.; Gu, Y. & Redfield, S. (1996). Doppler acoustic diagnostics of subsurface solar magnetic structure. *Astrophys. J.*, Vol. 470, 636–646

Moradi, H., Baldner, C.; Birch, A. C.; Braun, D. C.; Cameron, R. H.; Duvall, T. L.; Gizon, L.; Haber, D.; Hanasoge, S. M.; Hindman, B. W.; Jackiewicz, J.; Khomenko, E.; Komm, R.; Rajaguru, P.; Rempel, M.; Roth, M.; Schlichenmaier, R.; Schunker, H.; Spruit, H. C.; Strassmeier, K. G.; Thompson, M. J. & Zharkov, S. (2010). Modeling the subsurface structure of sunspots. *Solar Phys.*, Vol. 267, 1–73

Moradi, H.; Donea, A.-C.; Lindsey, C.; Besliu-Ionescu, D. & Cally, P. S. (2007). Helioseismic analysis of the solar flare-induced sunquake of 2005 January 15. *Min. Roy. Astron. Soc.* Vol. 374, 1155–1163

Quemerais, E. & Bertaux, J.-L. (2006). Retrieving the solar wind mass flux latitude and cycle dependence with SWAM/SOHO data. *Proc. COSPAR Sci. Assem.*, Vol. 36, 1615, Beijing

Roddier, F. (1975). Principe de réalisation d'un hologramme acoustique de lo surface du Soleil. *Comptes Rendus, Serie B—Sciences Physiques*, Vol. 281, 93–95

Rhodes, E. J.; Ulrich, R. & Simon, G. W. (1977). Observations of nonradial p-mode oscillations on the Sun. *Astrophys. J.*, Vol. 218, 901–919

Rhodes, E. J.; Deubner, F.-L. & Ulrich, R. (1979). A new technique for measuring solar rotation. *Astrophys. J.*, Vol. 227, 629–637

Scherrer, P. H.; Bogart, R. S.; Bush, R. I.; Hoeksema, J. T.; Kosovichev, A. G.; Schou, J.; Rosenberg, W.; Springer, L.; Tarbell, T. D.; Title, A.; Wolfson, C. J.; Zayer, I. & the MDI Engineering Team (1995). The Solar Oscillations Investigation—Michelson Doppler Imager *Solar Phys.*, Vol. 162, 129–188y

Schunker, H.; Braun, D. C.; Lindsey, C. & Cally, P. S. (2008). Physical properties of wave motion in inclined magnetic fields within sunspot penumbrae. *Solar Phys.*, Vol. 251, 341–359

Skartlien, R. (2001). Imaging of acoustic wave sources inside the Sun. *Astrophys. J.*, Vol. 554, 488–495

Skartlien, R. (2002). Local Helioseismology as an inverse source-inverse scattering problem. *Astrophys. J.*, Vol. 565, 1348–1365

Spruit, H. C. & Bogdan, T. J. (1992). The conversion of p-modes to slow modes and the absorption of acoustic waves by sunspots. *Astrophys. J. Letters*, Vol. 391, 109–112

Stein, R. F.; Bogdan, T. J.; Carlsson, M.; Hansteen, V; McMurry, A; Rosenthal, C. S. & Nordlund, A . (2004). Theory and simulations of solar atmospheric dynamics. A joint view from SOHO and TRACE. Proc. SOHO13 Conference. *Waves, Oscillations and Small-scale Events in the Solar Atmosphere*, pp. 93–105, Palma de Mallorca, Balearic Islands (Spain), September–October 2003, ESA SP-547

Ulrich, R. (1970). The five-minute oscillations on the solar surface. *Astrophys. J.*, Vol. 162, 993–1002

Zernike, F. (1938). The concept of degree of coherence and its application to optical problems. *Physica*, Vol. 5, 785–795

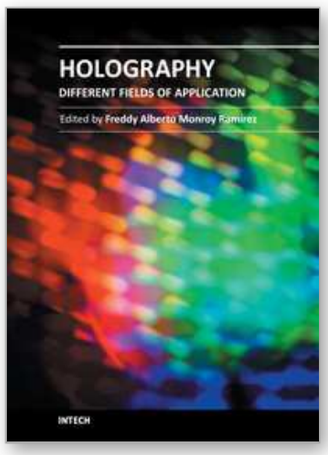

Holography - Different Fields of Application

Edited by Dr. Freddy Monroy

ISBN 978-953-307-635-5
Hard cover, 148 pages
Publisher InTech
Published online 12, September, 2011
Published in print edition September, 2011

This book depicts some differences from the typical scientific and technological literature on the theoretical study of holography and its applications. It offers topics that are not very commercial nor known, which will allow a different view of the field of optics. This is evident in chapters such as â€œElectron Holography of Magnetic Materialsâ€, â€œPolarization Holographic Gratings in Polymer Dispersed Formed Liquid Crystals, and â€œDigital Holography: Computer-generated Holograms and Diffractive Optics in Scalar Diffraction Domainâ€. The readers will gain a different view of the application areas of holography and the wide range of possible directions that can guide research in the fields of optics.

How to reference

In order to correctly reference this scholarly work, feel free to copy and paste the following:

Charles Lindsey, Douglas Braun, Irene González Hernández and Alina Donea (2011). Computational Seismic Holography of Acoustic Waves in the Solar Interior, Holography - Different Fields of Application, Dr. Freddy Monroy (Ed.), ISBN: 978-953-307-635-5, InTech, Available from: http://www.intechopen.com/books/holography-different-fields-of-application/computational-seismic-holography-of-acoustic-waves-in-the-solar-interior

INTECH
open science | open minds

InTech Europe
University Campus STeP Ri
Slavka Krautzeka 83/A
51000 Rijeka, Croatia
Phone: +385 (51) 770 447
Fax: +385 (51) 686 166
www.intechopen.com

InTech China
Unit 405, Office Block, Hotel Equatorial Shanghai
No.65, Yan An Road (West), Shanghai, 200040, China
中国上海市延安西路65号上海国际贵都大饭店办公楼405单元
Phone: +86-21-62489820
Fax: +86-21-62489821

IntechOpen